Available online at www.sciencedirect.com
ScienceDirect
Journal of Colloid and Interface Science 315 (2007) 721–730
JOURNAL OF Colloid and Interface Science
www.elsevier.com/locate/jcis

Diffusioosmotic flows in slit nanochannels

Shizhi Qian [a,*], Biswajit Das [b], Xiaobing Luo [c]

[a] Department of Mechanical Engineering, University of Nevada Las Vegas, 4505 Maryland Parkway, Las Vegas, NV 89154-4027, USA
[b] Department of Electrical and Computer Engineering, University of Nevada Las Vegas, 4505 Maryland Parkway, Las Vegas, NV 89154-4027, USA
[c] School of Energy and Power, Huazhong University of Science and Technology, Wuhan 430074, People's Republic of China

Received 5 May 2007; accepted 29 June 2007

Available online 24 August 2007

Abstract

Diffusioosmotic flows of electrolyte solutions in slit nanochannels with homogeneous surface charges induced by electrolyte concentration gradients in the absence of externally applied pressure gradients and potential differences are investigated theoretically. A continuum mathematical model consisting of the strongly coupled Nernst–Planck equations for the ionic species' concentrations, the Poisson equation for the electric potential in the electrolyte solution, and the Navier–Stokes equations for the flow field is numerically solved simultaneously. The induced diffusioosmotic flow through the nanochannel is computed as functions of the externally imposed concentration gradient, the concentration of the electrolyte solution, and the surface charge density along the walls of the nanochannel. With the externally applied electrolyte concentration gradient, a strongly spatially dependent electric field and pressure gradient are induced within the nanochannel that, in turn, generate a spatially dependent diffusioosmotic flow. The diffusioosmotic flow is opposite to the applied concentration gradient for a relatively low bulk electrolyte concentration. However, the electrolyte solution flows from one end of the nanochannel with a higher electrolyte concentration to the other end with a lower electrolyte concentration when the bulk electrolyte concentration is relatively high. There is an optimal concentration gradient under which the flow rate attains the maximum. The induced flow is enhanced with the increase in the fixed surface charge along the wall of the nanochannel for a relatively low bulk electrolyte concentration.

Keywords: Diffusioosmosis; Diffusioosmotic flow; Electrokinetics; Electrokinetic flow; Nanofluidics; Electrical double layer (EDL)

1. Introduction

In recent years, there has been a growing interest in developing nanofluidic devices with features comparable in size to DNA, proteins, and other biological molecules for biological and chemical analysis [1–5]. In nanofluidic devices, it is necessary to propel fluids from one part of the device to another, control fluid motion, enhance mixing, and separate fluids. Pressure-driven flow in nanochannels is usually very difficult due to its high pressure loss with a very low volume flow rate. On the other hand, electroosmotic pumps with no moving parts are commonly used to transport liquids through nanochannels by external electric fields. Electroosmosis and electrophoresis have been widely used for fluid and particle manipulations in microfluidics and nanofluidics. Instead of externally applying an electric field, an electrolyte solution in a nanochannel can also be driven by means of diffusioosmosis through the application of gradients of solute concentration. With a concentration gradient on the order of 1 M/cm along a charged surface with a zeta potential on the order of $k_B T/e$ (k_B is the Boltzmann constant, T is the absolute temperature, and e is the elementary charge), the induced diffusioosmotic flow has a velocity on the order of μm/s [6–17]. Like the well-known electroosmosis phenomenon, diffusioosmosis originates from electrostatic interaction between the electrolyte and the charged solid's surface that is in contact with the electrolyte solution. Therefore, both electroosmosis and diffusioosmosis fall into the same category of surface-driven phenomena that take advantage of the increase of surface to volume ratio [18]. However, flow generation in nanofluidics by diffusioosmosis has received less attention than fluid motion induced by electroosmosis.

We consider a nanochannel connecting two reservoirs on either side (Fig. 1). The wall of the nanochannel is charged. The

* Corresponding author.
E-mail address: shizhi.qian@unlv.edu (S. Qian).

0021-9797/$ – see front matter
doi:10.1016/j.jcis.2007.06.075

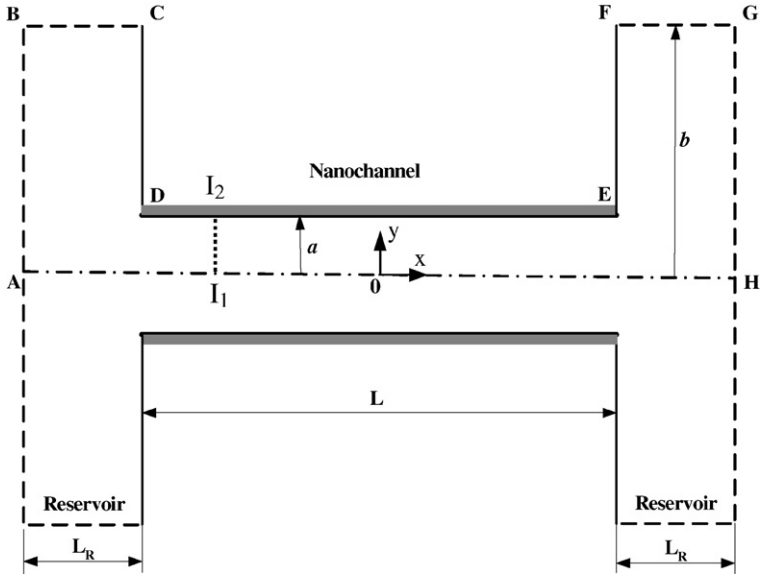

Fig. 1. Schematic of a slit nanochannel of length L and height $2a$ connecting two reservoirs on either side. The surface charge density along the wall of the nanochannel is σ_w. The length and height of the reservoir are, respectively, L_R and $2b$. When a concentration gradient of electrolyte solution is applied across the two reservoirs, a potential difference and a pressure gradient, and thus diffusioosmotic flow are induced in the absence of any external pressure gradient and potential difference.

two reservoirs contain a dilute electrolyte solution with different concentrations. Due to the electrostatic interaction between the ionic species present in the electrolyte solution and the fixed surface charge along the wall of the nanochannel, counterions accumulate in a thin liquid layer next to the solid's surface. This thin layer is known as the electrical double layer (EDL), and its thickness is typically on the order of 10 nm [19]. In the presence of an external concentration gradient of the electrolyte solution, fluid motion is generated by two mechanisms: electroosmotic and chemiosmotic effects. Due to the presence of the concentration gradient, electrolyte ions diffuse in the nanochannel, accompanied by a net diffusive flux of charge when the mobilities of the anion and cation are not equal. As a result, an electric field is induced that compensates for the net diffusive flux of charge across the nanochannel. The induced electric field, through its action on the counterions accumulated in the EDL, creates a body force that, in turn, induces fluid motion. In contrast to the electroosmotic flow driven by an externally applied electric field, the fluid motion due to the electroosmotic effect in diffusioosmosis phenomenon is driven by the induced electric field in the absence of an externally applied electric field. Although there is no externally applied pressure gradient across the channel, a pressure gradient is induced by the electrolyte gradient, which induces shear in the EDL and a flow opposite to the concentration gradient [6–18]. Therefore, the diffusioosmotic flow is driven by both the induced electric field and the induced pressure gradient in the absence of the externally applied electric field and pressure gradient. As compared to the electroosmotic flow and the pressure-driven flow, the two strategies, electroosmosis and pressure-driven, are synergetically combined in diffusioosmotic flow, yielding strongly enhanced interfacial driven flows in nanofluidic and microfluidic devices [18].

Previous investigations of diffusioosmotic flow are very limited. Most studies to date have focused on diffusioosmotic flows near plane walls and in straight conduits (i.e., capillary tubes and slits) with uniform zeta potentials or surface charges along the walls. See, for example, Keh and Ma [17] and the references cited therein. In addition, most previous analysis of diffusioosmotic flows has been subjected to several restrictions, such as a thin EDL [6,7], a sufficiently low zeta potential along the wall [8,13], and neglected effects of the ionic concentration distributions and ionic convection on the induced local electric field and pressure gradient [7,8,13,14]. Moreover, the deformation and concentration polarization of the EDL due to the convection have not been taken into account in previous work. In this paper, we study diffusioosmotic flows in slit nanochannels with uniform surface charge densities along the channel's walls. In contrast to the previous work, the current analysis accounts for the polarization of the EDL with no assumption made concerning the thickness of the EDL and the magnitude of the zeta potential or surface charge density along the wall. In addition, the effects of the reservoirs connecting the nanochannel are also taking into account in the current work.

The rest of the paper is organized as follows. Section 2 describes the full mathematical model for the fluid motion induced by both the induced pressure gradient and the induced electric field and the general multi-ion mass transport model that accounts for the polarization of the EDL. Detailed code validation is described in Section 3. The diffusioosmotic flows in slit nanochannels under various conditions are presented and discussed in Section 4. Section 5 concludes.

2. Mathematical model

Let us consider a charged slit nanochannel with length L and height $2a$ connecting two identical reservoirs on either side. Fig. 1 schematically depicts the geometry. The length and height of the reservoir are, respectively, L_R and $2b$. We assume

that the top and bottom walls of the nanochannel carry the same surface charge density, σ_w. Utilizing the symmetry of the geometry, a two-dimensional Cartesian coordinate system (x, y) with origin located at the center of the nanochannel is used. The x and y coordinates are, respectively, parallel and perpendicular to the axis of the nanochannel. The symmetrical model geometry is represented by the region bounded by the outer boundary ABCDEFGH and the line of symmetry, AH. The dashed line segments, AB, BC, FG, and GH, represent the regions in the reservoirs. The length L_R and height $2b$ of the reservoir are sufficiently large to ensure that the electrochemical properties at the locations of AB, BC, FG, and GH are not influenced by the nanochannel. We assume that the walls of the two reservoirs (line segments CD and EF) are electrically neutral surfaces. The left and right reservoirs are filled with two identical electrolyte solutions with different bulk concentrations, C_L and C_R, and we assume that $C_R > C_L$ so that a concentration gradient along the x-direction is externally imposed. We also assume that there is no externally applied pressure gradient across the two reservoirs.

Recently, Qian et al. [20] and Liu et al. [21] studied DNA's electrophoretic motion through a nanopore using a continuum model consisting of the Nernst–Planck equations for the concentrations of the ionic species, the Poisson equation for the electrical potential in the electrolyte solution, and the Navier–Stokes equations for the flow field. The theoretical predictions agree qualitatively with the experimental data obtained from the literature and the predictions obtained from the molecular dynamics simulations pertaining to the translocation of DNA molecules in nanopores. We therefore assume that the continuum model is still valid for our current analysis. In the following sections, we present dimensional mathematical models for the fluid motion and ionic mass transport through the reservoirs and the nanochannel.

2.1. The mathematical model for the fluid motion

We consider a binary, symmetric electrolyte solution such as KCl aqueous solution. Because typically the Reynolds numbers of the diffusioosmotic flows in nanochannels are very small, we neglect the inertial terms in the Navier–Stokes equations and model the fluid motion with the Stokes equations. Subsequently, the motion of the incompressible electrolyte solution generated by the induced electrostatic force and the induced pressure gradient is described by the modified Stokes equations

$$\nabla \cdot \mathbf{u} = 0 \tag{1}$$

and

$$-\nabla p + \mu \nabla^2 \mathbf{u} - F(z_1 c_1 + z_2 c_2)\nabla V = 0. \tag{2}$$

In the above, $\mathbf{u} = u_x \mathbf{e}_x + u_y \mathbf{e}_y$ is the fluid's velocity. Hereafter, bold letters denote vectors; $\mathbf{e}_x$ and $\mathbf{e}_y$ are, respectively, unit vectors in the x- and y-directions; u_x and u_y are, respectively, the velocity components in the x- and y-directions; p is the pressure; V is the electric potential in the electrolyte solution; c_1 and c_2 are, respectively, the molar concentrations of the positive (K^+) and negative (Cl^-) ions in the electrolyte solution; z_1 and z_2 are, respectively, the valences of the positive and negative ions; F is the Faraday constant; and μ is the electrolyte solution's dynamic viscosity. The last term on the left-hand side of Eq. (2) represents the electrostatic force through the interaction between the induced electric field and the net charge density in the electrolyte solution, which plays a similar role to that of the induced pressure gradient (the first term on the LHS of Eq. (2)).

In order to solve Eqs. (1) and (2), appropriate boundary conditions are required. A nonslip boundary condition (i.e., $u_x = u_y = 0$) is specified at the solid walls of the nanochannel and the reservoirs (line segments CD, DE, and EF in Fig. 1). At the planes AB and GH of the reservoirs, since they are far away from the nanochannel and there is no externally applied pressure gradient across the two reservoirs, normal pressure with $p = 0$ is used in the planes AB and GH. A symmetric boundary condition is used along the line of symmetry, AH. Finally, slip boundary conditions are used on the segments BC and FG, since they are far away from the entrances of the nanochannel.

2.2. The general model for multi-ion mass transport

2.2.1. Governing equations

In this section, we present a more general multi-ion mass transport model that includes the Nernst–Planck equation for the concentration of each ionic species and the Poisson equation for the electric potential in the electrolyte solution. The flux density of each aqueous species due to convection, diffusion, and migration is given by

$$\mathbf{N}_k = \mathbf{u}c_k - D_k \nabla c_k - z_k m_k F c_k \nabla V, \quad k = 1 \text{ and } 2. \tag{3}$$

In the above, c_k is the molar concentration; D_k is the diffusion coefficient; z_k is the valence; and m_k is the mobility of the kth ionic species. The flow field $\mathbf{u}$ is determined by simultaneously solving the continuity and the Stokes equations (1) and (2). The first, second, and third terms on the RHS of expression (3) represent, respectively, the convective, diffusive, and migrative flux density. Using the Nernst–Einstein relation, the mobility m_k is expressed in terms of the diffusivity D_k, the universal gas constant R, and the absolute temperature T:

$$m_k = \frac{D_k}{RT}, \quad k = 1 \text{ and } 2. \tag{4}$$

Under steady state, the concentration of each species is governed by the Nernst–Planck equation:

$$\nabla \cdot \mathbf{N}_k = 0, \quad k = 1 \text{ and } 2. \tag{5}$$

The set of Eq. (5) consists of three unknown variables: the concentrations of the positive and negative ions and the electrical potential, V. The Poisson equation provides the third equation:

$$-\varepsilon \nabla^2 V = F(z_1 c_1 + z_2 c_2). \tag{6}$$

In the above, ε is the permittivity of the electrolyte solution.

2.2.2. Boundary conditions for the Nernst–Planck equations

In the plane AB, the concentrations of the positive and negative ions are the same as the bulk concentration of the electrolyte solution present in the left reservoir:

$$c_1 = c_2 = C_L \quad \text{in the plane AB.} \tag{7}$$

Similarly, the concentrations of the ions at the plane GH are the same as the bulk concentration of the electrolyte solution in the right reservoir:

$$c_1 = c_2 = C_R \quad \text{in the plane GH.} \tag{8}$$

At the walls of the reservoirs and the wall of the nanochannel (line segments CD, DE, and EF in Fig. 1), since the solid surfaces are impervious to ions, the net ion fluxes normal to the rigid walls are zero:

$$\mathbf{n}\cdot\mathbf{N}_1 = \mathbf{n}\cdot\mathbf{N}_2 = 0 \quad \text{in the planes CD, DE, and EF.} \tag{9}$$

In the above, $\mathbf{n}$ is the unit vector normal to the corresponding surface.

The boundary conditions on the segments BC and FG are defined with the assumption that these surfaces are in the bulk electrolyte reservoirs. Accordingly, zero normal flux is used for the Nernst–Planck equations:

$$\mathbf{n}\cdot\mathbf{N}_1 = \mathbf{n}\cdot\mathbf{N}_2 = 0 \quad \text{in the planes BC and FG.} \tag{10}$$

Along the segment AH, a symmetric boundary condition is used for the Nernst–Planck equations:

$$\mathbf{n}\cdot\mathbf{N}_1 = \mathbf{n}\cdot\mathbf{N}_2 = 0 \quad \text{in the plane AH.} \tag{11}$$

2.2.3. Boundary conditions for the Poisson equation

A symmetric boundary condition for the electric potential in the electrolyte solution is used in the plane AH:

$$\mathbf{n}\cdot\nabla V = 0 \quad \text{in the plane AH.} \tag{12}$$

Along the plane AB, the boundary condition for the electric potential is

$$V = \phi \quad \text{in the plane AB} \tag{13}$$

and the potential, ϕ, is unknown a priori and needs to be determined from the zero current condition:

$$\int_S F(z_1\mathbf{N}_1 + z_2\mathbf{N}_2)\cdot\mathbf{n}\,dS = 0. \tag{14}$$

In the above, S is the surface area of the plane AB. The current density in the electrolyte solution is

$$\mathbf{i} = F(z_1\mathbf{N}_1 + z_2\mathbf{N}_2). \tag{15}$$

Based on the Nernst–Planck equation (5), one can obtain the conservation of charge:

$$\nabla\cdot\mathbf{i} = 0. \tag{16}$$

At any cross section (i.e., $I_1 - I_2$ in Fig. 1) that is perpendicular to the x-axis, we choose a control volume that is bounded by the planes AB, BC, CD, DI_2, I_2I_1, and AI_1. Based on the boundary conditions (9)–(11), the currents entering the control volume through the planes BC, CD, DI_2, and AI_1 are zero. Constraint (14) implies that the current entering the control volume through the surface AB is zero. Based on the conservation of charge (14), the current along the cross section I_1I_2 is zero. Therefore, constraint (14) implies that the current is zero for each cross section that is perpendicular to the x-axis.

Along the plane GH, we set the potential to zero as the reference potential:

$$V = 0 \quad \text{in the plane GH.} \tag{17}$$

Since the surfaces of BC and FG are far away from the nanochannel and are in the bulk electrolyte reservoirs, no charge boundary condition for the potential is used:

$$\mathbf{n}\cdot\nabla V = 0 \quad \text{in the planes BC and FG.} \tag{18}$$

Since the walls of the reservoirs (planes CD and EF) do not carry a fixed charge, we use

$$\mathbf{n}\cdot\nabla V = 0 \quad \text{in the planes CD and EF.} \tag{19}$$

Along the wall of the nanochannel, the following boundary condition for the potential is used:

$$\mathbf{n}\cdot(-\varepsilon\nabla V) = \sigma_w \quad \text{in the plane DE.} \tag{20}$$

The above model differs from the previous study on diffusioosmosis of electrolyte solutions in a fine capillary tube [17], in which the ionic concentration of each species is described by the Boltzmann distribution and the electrical potential is then described by the commonly used Poisson–Boltzmann model. Consequently, the electrostatics and hydrodynamics are decoupled. However, the Boltzmann distribution is valid under the following assumptions: (a) the system is in equilibrium (i.e., no convection and diffusion); (b) the channel wall has a homogeneous surface charge; and (c) the charged surface is in contact with an infinitely large liquid medium where the potential is zero and the ionic concentration is the same as that of the bulk solution [22, pp. 13–14]. In the current study, the liquid is confined in a nanochannel with dimensions comparable to the thickness of the EDL. Obviously, the Boltzmann distribution is not valid in our case. The multi-ion model presented here accounts for the deformation and polarization of the EDL and is valid for any thickness of the EDL. Witness that the momentum and mass transport equations are strongly coupled. The flow field affects the mass transport due to convection. On the other hand, the mass transport, in turn, affects the flow field through the induced electric field. The model requires one to simultaneously solve the coupled equations including the Stokes equations (1) and (2), the Nernst–Planck equation (5), and the Poisson equation (6).

3. Code validation

We solved the strongly coupled system with the commercial finite element package COMSOL (version 3.3a, www.femlab.com) operating with a 64-bit dual-processor workstation with 32 GB RAM. The computational domain bounded by ABCDEFGH in Fig. 1 was discretized into quadrilateral elements since

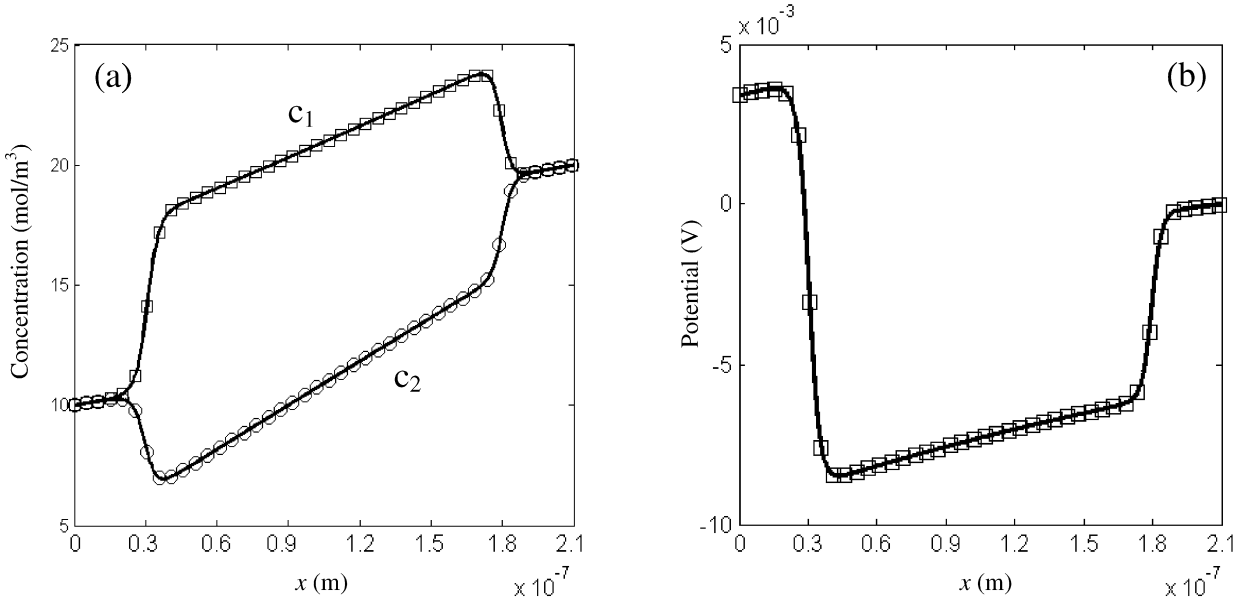

Fig. 2. (a) Concentrations of the positive (c_1) and negative (c_2) ions along the x-axis of the nanochannel. (b) The induced electric potential along the x-axis. The lines and symbols represent, respectively, our numerical results and those obtained by Pivonka and Smith [25].

the domain is fairly regular in shape. We employed nonuniform elements with a larger number of elements within the nanochannel with at least 10 elements positioned inside the EDL next to the wall (segment DE) of the nanochannel. We compared the solutions obtained for different mesh sizes to ensure that the numerical solutions are convergent, independent of the size of the finite elements, and satisfy the various conservation laws.

We first validated the numerical solutions of the conjugated problems when the flows are driven by electroosmosis alone. First, we simulated an electroosmotic flow within a cylindrical microchannel without connecting reservoirs on either side. Note that the geometry of this case is different from that shown in Fig. 1. We also assume that the wall of the microchannel has a constant zeta potential and the axial electric field is uniform within the microchannel. The numerical results agree very well with those obtained from the analytical solution provided by Li [22] and derived within the Debye–Hückel limit valid for sufficiently low zeta potentials. Second, we simulated the ionic mass transport in nanofluidic channels without considering the convection (i.e., $\mathbf{u} = 0$). In other words, the ionic mass transport is governed only by the diffusive and migrative processes. We solved the set of Nernst–Planck equations (5) without convection and the Poisson equation (6), and our numerical results agree well with those obtained from Daiguji et al. [23]. Third, we simulated the full mathematical model including the fluid motion and the ionic mass transport in a rectangular nanochannel without connecting reservoirs on either side. The height and length of the channel are, respectively, 100 nm and 5 μm. The fluid motion is driven by electroosmosis through the externally applied electric field. Our results obtained from the commercial software COMSOL are in excellent agreement with the results of Theemsche et al. [24], who numerically solved the same problem with their own finite element code written in C++.

We also simulated the diffusioosmotic flow in a slit nanochannel when $L = 150$ nm, $a = 5$ nm, $L_R = 30$ nm, $b = 15$ nm, $C_L = 10$ mM, $C_R = 20$ mM, and $\sigma_w = -0.01$ C/m^2. This problem has been investigated by Pivonka and Smith [25] during the study of nanoscale electrohydrodynamic transport phenomena in charged porous materials (see subproblem 1.1, row 4 in Table II, page 1984 in Ref. [25]). Fig. 2a depicts the concentration distributions of the positive ions (c_1) and negative ions (c_2) along the x-axis of the channel when $D_2 = 2D_1 = 3.0 \times 10^{-9}$ m^2/s. Fig. 2b depicts the induced electric potential along the x-axis. The lines and symbols in Figs. 2a and 2b represent, respectively, our numerical results and the results obtained by Pivonka and Smith, and they are in excellent agreement. The potentials ϕ obtained from our numerical simulation and the result by Pivonka and Smith are, respectively, 3.4 and 3.2 mV, and they are in good agreement. As compared to the work by Pivonka and Smith, the current study systematically investigated the diffusioosmotic flows in nanochannels as functions of the externally imposed concentration gradient, the concentration of the electrolyte solution, and the surface charge along the walls of the nanochannel, which have not been investigated by Pivonka and Smith.

4. Results and discussions

In this section, we present a few numerical results of the diffusioosmotic flows in slit nanochannels with various homogeneous surface charge densities using the general multi-ion model. We focus on the effects of the bulk electrolyte concentration in the left reservoir, C_L, the magnitude of the concentration gradient, $(C_R - C_L)/(L + 2L_R)$, and the magnitude of the surface charge density along the wall of the nanochannel on the induced fluid motion. In the numerical simulations, a nanochannel with length $L = 1.0$ μm and height $2a = 20$ nm connecting two identical reservoirs 0.2×0.2 μm^2 (i.e., $L_R = 0.2$ μm and $2b = 0.2$ μm) in size on either side of the nanochannel. The temperature of the electrolyte solution in the reservoirs and

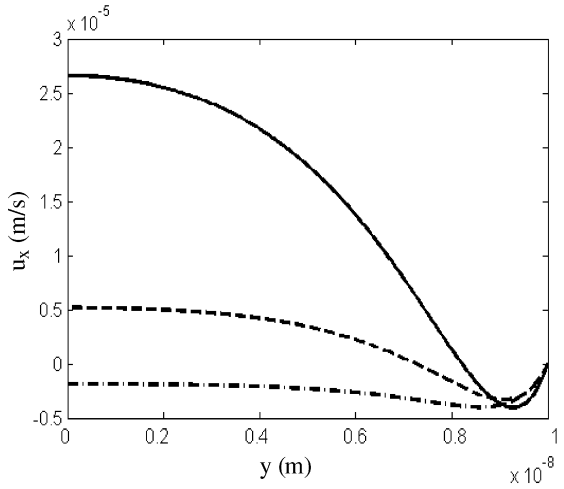

Fig. 3. The x-component diffusioosmotic velocity as a function of y at the cross section $x = 0$ when the electrolyte concentration in the left reservoir is, respectively, $C_L = 10$ mM (solid line), 20 mM (dashed line), and 30 mM (dash–dotted line). $\Delta C = 10$ mM and $\sigma_w = -0.01$ C/m^2.

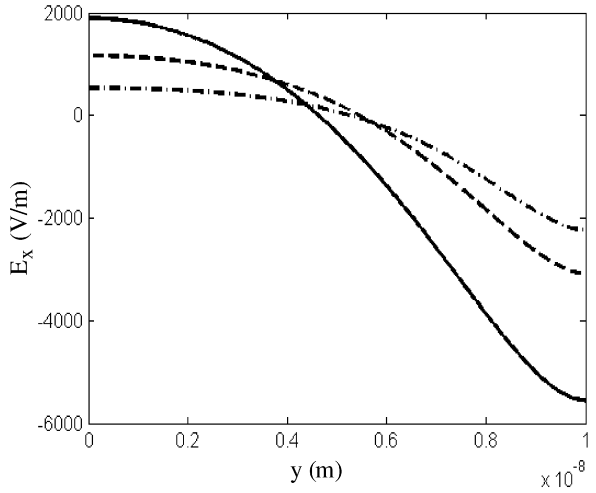

Fig. 4. The electric field in the x-direction as a function of y at the cross section $x = 0$ when the electrolyte concentration in the left reservoir is, respectively, $C_L = 10$ mM (solid line), 20 mM (dashed line), and 30 mM (dash–dotted line). $\Delta C = 10$ mM and $\sigma_w = -0.01$ C/m^2.

the nanochannel is 300 K. The diffusion coefficients of the ions K^+ (c_1) and Cl^- (c_2) are, respectively, 1.95×10^{-9} and 2.03×10^{-9} m^2/s.

4.1. *Effects of the bulk electrolyte concentration* C_L

Fig. 3 depicts the x-component velocity profiles, $u_x(0, y)$, in the central cross section ($x = 0$) of the nanochannel when the surface charge density is $\sigma_w = -0.01$ C/m^2. The solid, dashed, and dash–dotted lines correspond, respectively, to the cases with $C_L = 10$, 20, and 30 mM with $\Delta C = C_R - C_L = 10$ mM. The electrolyte concentration gradient is in the negative x-direction. When C_L is below a threshold value, the fluid flows in the direction opposite to the electrolyte concentration gradient in the central region of the nanochannel and u_x is negative in the region near the wall. As C_L increases, the magnitude of the positive velocity in the central region of the nanochannel decreases. Once the bulk electrolyte concentration, C_L, is above a critical value, the x-component velocity becomes negative in the entire nanochannel, which indicates that the fluid flows from the right reservoir with a higher electrolyte concentration toward the left reservoir with a lower electrolyte concentration. The velocity profile is different from the "pluglike" velocity profile as typically encountered in the electroosmotic flow in a nanochannel with a homogeneous surface charge density. The velocity profile in the diffusioosmotic flow results from the combination of the electroosmotic flow and the pressure-driven flow.

To better understand the reasons for the diverse flow directions, Fig. 4 depicts the induced electric field in the x-direction along the cross section $x = 0$ when the surface charge density is $\sigma_w = -0.01$ C/m^2. In contrast to the electroosmotic flow, in which the axial electric field is almost uniform along the cross sections, which are perpendicular to the flow direction, the induced axial electric field in the diffusioosmotic flow is spatially dependent. The direction of the x-component electric field is opposite to the electrolyte concentration gradient in the central region of the channel, and is in the same direction as that of the electrolyte concentration gradient in the region near the wall of the channel. As the bulk electrolyte concentration, C_L, increases, the magnitude of the electric field decreases. Since the wall of the nanochannel carries negative surface charges, the concentration of the counterions (K^+) is enriched and the concentration of the co-ions (Cl^-) is depleted inside the nanochannel. As a result, the net charge density, $\rho_e = F(z_1c_1 + z_2c_2)$, is positive. Through the interaction between the net charge density and the induced axial electric field, the fluid moves in the positive x-direction in the central region of the channel in which the axial electric field is positive, and the fluid velocity is negative in the region near the wall of the channel in which the axial electric field is negative.

Besides the electrostatic force, the fluid is also driven by the induced pressure gradient. Fig. 5 depicts the pressure gradient in the x-direction, $\partial p/\partial x$, along the cross section $x = 0$ when the surface charge density is $\sigma_w = -0.01$ C/m^2. All other conditions are the same as those in Fig. 3. A negative pressure gradient is induced for various bulk electrolyte concentrations. In the central region of the channel, the magnitude of the pressure gradient is relatively low. The magnitude of the pressure gradient increases until it peaks and then declines as y increases. The magnitude of the induced pressure gradient decreases as the concentration, C_L, increases. The fluid driven by the induced negative pressure gradient flows in the positive x-direction. The net flow as shown in Fig. 3 is the combined result of the flows driven by the induced electrostatic force and the induced pressure gradient. In the central region of the channel, the net flow is positive since the flow is driven by favorable electrostatic force and pressure gradient. In the region near the wall, the flow driven by the favorable pressure gradient is in the positive x-direction. However, the negative axial electric field (Fig. 4) drives the counterions and their surrounding liquid molecules to move in the negative x-direction. In the region near the wall, the flow driven by the electrostatic force is opposite to the pressure-driven flow, and the former is dominant. As a result, the net flow in the region near the wall is in the negative x-direction.

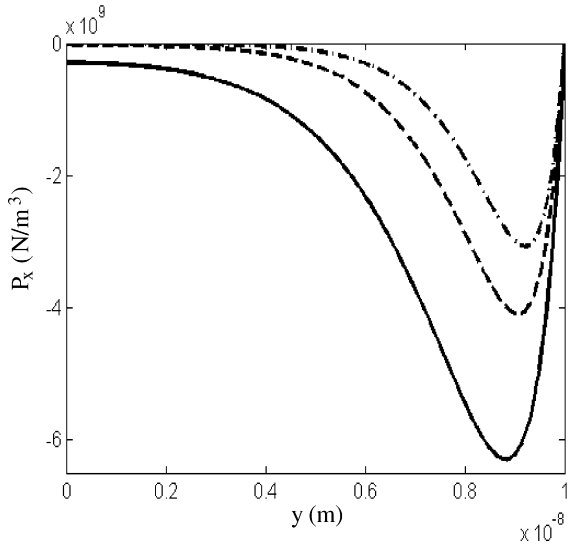

Fig. 5. The pressure gradient in the x-direction as a function of y at the cross section $x = 0$ when the electrolyte concentration in the left reservoir is, respectively, $C_L = 10$ mM (solid line), 20 mM (dashed line), and 30 mM (dash–dotted line). $\Delta C = 10$ mM and $\sigma_w = -0.01$ C/m^2.

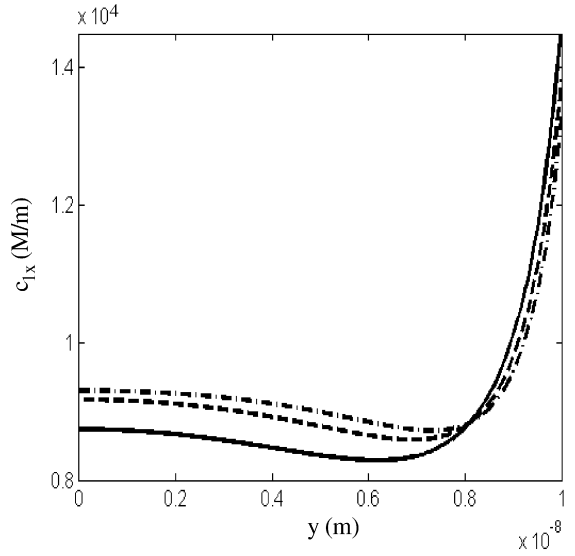

Fig. 6. The concentration gradient of the ions K^+ in the x-direction as a function of y at the cross section $x = 0$ when the electrolyte concentration in the left reservoir is, respectively, $C_L = 10$ mM (solid line), 20 mM (dashed line), and 30 mM (dash–dotted line). $\Delta C = 10$ mM and $\sigma_w = -0.01$ C/m^2.

To explain the spatial dependence of the induced electric field and diffusioosmotic flow, Figs. 6 and 7 depict, respectively, the concentration gradients of the ions K^+ (c_1) and the ions Cl^- (c_2) in the x-direction when the surface charge density is $\sigma_w = -0.01$ C/m^2. Due to the interaction between the fixed negative surface charge along the wall of the nanochannel and the ionic species in solution, the counterions (K^+) are enriched and the co-ions (Cl^-) are depleted near the wall of the nanochannel where the EDL is expected to be present. Note that the local electroneutrality condition, $z_1c_1 + z_2c_2 = 0$, is not valid, even along the centerline ($y = 0$) of the nanochannel. Since the net charge density, $\rho_e = F(z_1c_1 + z_2c_2)$, in the centerline is not zero, the boundary condition in the bulk solution is different from that used during the derivation of the Boltzmann distribution. Consequently, the Boltzmann distribution is therefore no longer valid [22, p. 15]. In the central region of the channel, the variations of $\partial c_1(0, y)/\partial x$ and $\partial c_2(0, y)/\partial x$ with y are not significant. In the region near the wall of the channel, the concentration gradient of the K^+ ions exponentially increases as y approaches the negatively charged wall of the channel. In contrast, the concentration gradient of the ions Cl^- exponentially decreases as y increases in the region near the wall since the wall is negatively charged. As the concentration C_L increases while keeping the concentration gradient and the surface charge density σ_w constant, the x-component concentration gradient of the ions K^+ increases in the central region of the channel and slightly decreases in the region near the wall (Fig. 6). However, as the concentration C_L increases, the x-component concentration gradient of the ions Cl^- decreases in the central region and increases in the region near the wall of the channel (Fig. 7). Fig. 8 depicts the local diffusive flux density in the x-direction, $J_D = D_2\partial c_2/\partial x - D_1\partial c_1/\partial x$, as a function of y, and all other conditions are the same as those in Fig. 6. In the central region of the channel, the diffusive flux density is positive and decreases as the bulk concentration C_L increases. The net diffusive flux density in the x-direction becomes negative and its amplitude decreases as the bulk concentration C_L increases in the region near the wall of the nanochannel. The spatially dependent diffusive flux density induces spatially dependent velocity and electric field so that the total current across the cross section $x = 0$ is zero. For a relatively low bulk concentration C_L, the x-component convective flux density, $J_C = u_x(c_1 - c_2)$, and migrative flux density, $J_M = -(z_1^2D_1c_1 + z_2^2D_2c_2)\frac{F}{RT}\frac{\partial V}{\partial x}$, are positive in the central region of the channel, in which both the x-component velocity and electric field are positive. In the region near the wall of the channel, the x-component diffusive flux density (J_D), the convective flux density (J_C), and the migrative flux density (J_M)

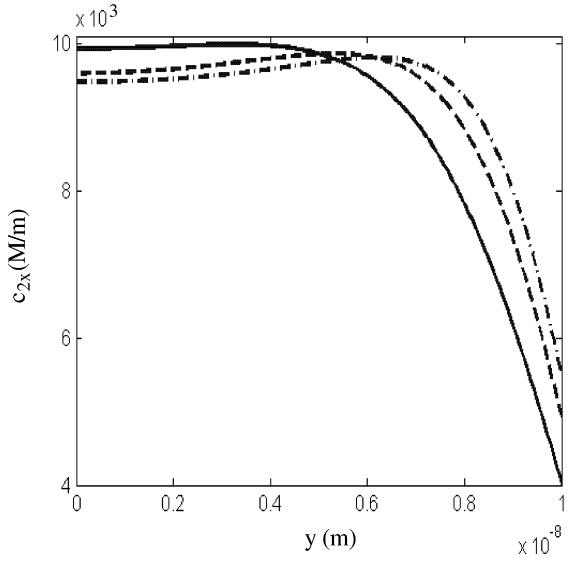

Fig. 7. The concentration gradient of the ions Cl^- in the x-direction as a function of y at the cross section $x = 0$ when the electrolyte concentration in the left reservoir is, respectively, $C_L = 10$ mM (solid line), 20 mM (dashed line), and 30 mM (dash–dotted line). $\Delta C = 10$ mM and $\sigma_w = -0.01$ C/m^2.

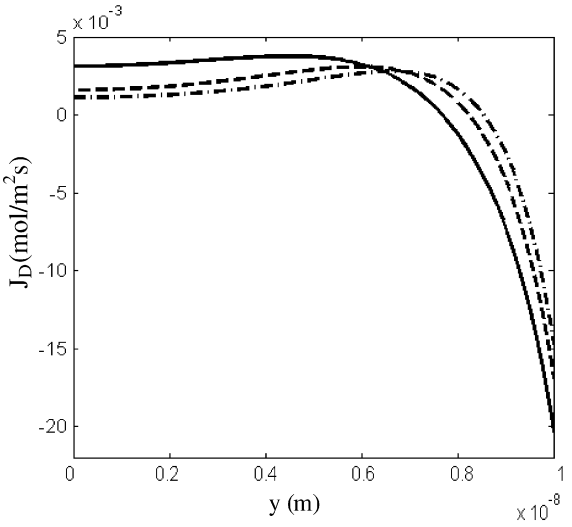

Fig. 8. The local diffusive flux density in the x-direction, $J_D = D_2\partial c_2/\partial x - D_1\partial c_1/\partial x$, as a function of y at the cross section $x = 0$ when the electrolyte concentration in the left reservoir is, respectively, $C_L = 10$ mM (solid line), 20 mM (dashed line), and 30 mM (dash–dotted line). $\Delta C = 10$ mM and $\sigma_w = -0.01$ C/m^2.

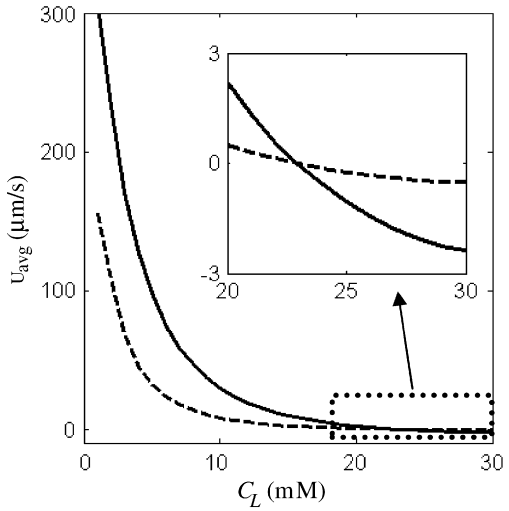

Fig. 9. The cross-sectional average velocity, $U_{avg} = \frac{1}{a}\int_0^a u_x(0, y)\,dy$, as a function of the bulk electrolyte concentration C_L when $\Delta C = 10$ mM, $\sigma_w = -0.01$ C/m^2 (solid line), and $\sigma_w = -0.005$ C/m^2 (dashed line).

are negative. The total current, $I = F\int_0^a (J_C + J_D + J_M)\,dy$, at the cross section $x = 0$ is zero. As the bulk concentration C_L increases, the magnitude of the diffusive flux density decreases (Fig. 8). As a result, lower flow velocity u_x and electric field in the x-direction are generated to induce lower convective and migrative currents in order to compensate for the net diffusive current. When C_L exceeds a certain threshold value, the x-component velocity and thus J_C become negative so as to compensate for the net results of J_D and J_M in the nanochannel.

Fig. 9 depicts the cross-sectional average velocity, $U_{avg} = \frac{1}{a}\int_0^a u_x(0, y)\,dy$, as a function of the bulk electrolyte concentration C_L when $\Delta C = 10$ mM. The small figure within Fig. 9 shows the details in the range of $20 \leqslant C_L \leqslant 30$ mM. The solid and dashed lines in Fig. 9 represent, respectively, the cases of $\sigma_w = -0.01$ and -0.005 C/m^2. When the bulk electrolyte concentration is relatively low, the cross-sectional average velocity or flow rate decreases as C_L increases. The results imply that one can enhance the flow by using a lower bulk electrolyte concentration in the left reservoir while externally applying the same concentration gradient. When the bulk concentration C_L is above a certain value, the average velocity or flow rate decreases only slightly as the bulk electrolyte concentration C_L increases. For a relatively high bulk concentration C_L, the direction of the net flow is reversed and the fluid is pumped from the reservoir with a higher concentration to the other with a lower concentration.

4.2. *Effect of the concentration gradient*

By keeping all conditions the same, one can vary the concentration gradient by changing the concentration difference, ΔC, or the bulk electrolyte concentration in the right reservoir, C_R. Fig. 10 depicts the x-component velocity profile, $u_x(0, y)$, as a function of y at the cross section $x = 0$ when the surface charge density $\sigma_w = -0.01$ C/m^2, $C_L = 10$ mM, and the concentration difference $\Delta C = 10$ mM (solid line), 20 mM (dashed line), and 40 mM (dash–dotted line). The fluid moves in the direction opposite to the externally applied concentration gradient in the central region of the channel, and flows in the same direction as that of the concentration gradient in the region near the wall of the channel for various concentration gradients. For a relatively small concentration gradient applied across the nanochannel, the positive flow in the central region and the negative flow in the region near the wall of the channel are enhanced as the concentration gradient increases. The primary reason for the enhancement of the flow with the increase in the concentration gradient is that a higher, negative diffusive current is induced that requires increased positive migrative and convective currents to compensate for the diffusive current so that the net current is zero in the system. When the concentration gradient is relatively large, as the concentration gradient increases further, the central region with a positive flow velocity shrinks and the region with a negative flow velocity expands. The flow in the region with a negative flow velocity is enhanced and the flow in the central region is reduced with the increase in the concentration gradient. This behavior can be explained as follows. The net charge density, $\rho_e = F(z_1c_1 + z_2c_2)$, decreases in the central region, and increases in the region near the wall of the channel with the increases in ΔC (results are not shown here). The distributions of the electric field in the x-direction under various concentration gradients are similar to that shown in Fig. 4. The magnitudes of the positive electric field in the central region and the negative electric field in the region near the wall increase as ΔC increases (results are not shown here). Therefore, the negative electrostatic force in the region near the wall increases with the increase in ΔC. However, the positive electrostatic force in the central region slightly decreases as ΔC increases due to the decrease in the net charge density. Therefore, the negative flow in the region near the wall is enhanced and the positive flow in the central region is reduced. Consequently, the cross-sectional average velocity decreases with the increase in the concentration difference or concentra-

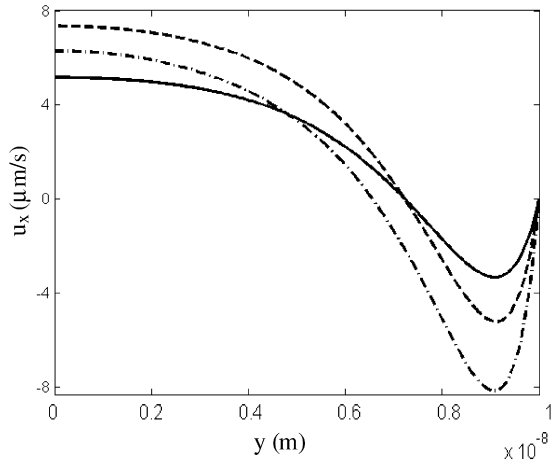

Fig. 10. The x-component diffusioosmotic velocity as a function of y at the cross section $x = 0$. $C_L = 10$ mM, $\sigma_w = -0.01$ C/m^2, and $\Delta C = 10$ mM (solid line), 20 mM (dashed line), and 40 mM (dash–dotted line).

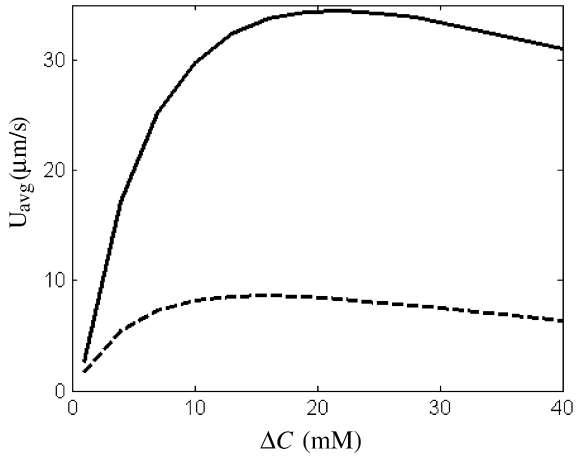

Fig. 11. The cross-sectional average velocity as a function of the bulk concentration difference, $\Delta C = C_R - C_L$, when $C_L = 10$ mM, $\sigma_w = -0.01$ C/m^2 (solid line), and $\sigma_w = -0.005$ C/m^2 (dashed line).

tion gradient when the latter is relatively high. Fig. 11 depicts the cross-sectional average velocity as a function of ΔC when $C_L = 10$ mM and the surface charge densities are, respectively, $\sigma_w = -0.01$ C/m^2 (solid line) and -0.005 C/m^2 (dashed line). When the bulk concentration difference or the axial concentration gradient is relatively small, the average velocity or flow rate nonlinearly increases as ΔC increases. As the bulk electrolyte concentration difference or the concentration gradient increases further, the flow rate attains a maximum at the concentration difference ΔC_{opt} and then slightly decreases. The results imply that there is an optimal concentration gradient to achieve the maximum flow rate. The optimal concentration difference, ΔC_{opt}, depends on the level of the surface charge density along the wall of the channel. The value of ΔC_{opt} in a nanochannel with a higher surface charge density is larger than that in a channel with a lower surface charge density.

4.3. Effect of the surface charge density along the nanochannel's wall

Fig. 9 depicts the cross-sectional average velocity as a function of the bulk concentration C_L under two different surface charge densities while keeping all other conditions the same. For a relatively low C_L, the flow rate is significantly enhanced in a channel with a higher surface charge density. However, when the bulk concentration C_L is relatively high, the effect of the surface charge density on the flow rate is not significant. Fig. 11 depicts the cross-sectional average velocity as a function of the bulk concentration difference when $C_L = 10$ mM, $\sigma_w = -0.01$ C/m^2 (solid line) and -0.005 C/m^2 (dashed line). Under all other identical conditions, the flow rate is higher in a nanochannel carrying a higher surface charge density since the interaction between the fixed surface charge along the wall and the mobile charges in the electrolyte solution increases as the surface charge density increases. As the fixed surface charge density increases, more counterions (K^+) are attracted to the negatively charged wall, and more co-ions (Cl^-) are repelled from the negatively charged wall and are depleted from

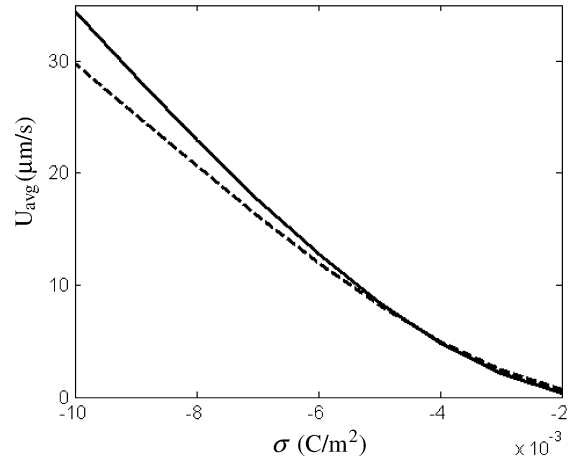

Fig. 12. The cross-sectional average velocity as a function of the surface charge density when $C_L = 10$ mM, $\Delta C = 20$ mM (solid line), and $\Delta C = 10$ mM (dashed line).

the nanochannel. The diffusive current increases with the increase in the fixed surface charge along the wall leading to higher electric field and migrative current so as to compensate for the diffusive current. Consequently, a higher flow rate is induced as the magnitude of the surface charge density increases. Fig. 12 depicts the cross-sectional average velocity as a function of the fixed charge density along the wall of the channel when $C_L = 10$ mM, $\Delta C = 10$ mM (dashed line), and $\Delta C = 20$ mM (solid line). Under all other identical conditions, the cross-sectional average velocity increases with the magnitude of the surface charge density.

5. Conclusions

The diffusioosmotic flows in slit nanochannels connecting reservoirs on either side have been studied theoretically with the general multi-ion mass transport model taking into account of the distortion and polarization of the EDLs adjacent to the charged wall of the nanochannel. Despite the zero potential and pressure differences externally applied between the reservoirs

connected on either end of the nanochannel, a spatially dependent electric field and a pressure gradient are induced by the variations of the electrolyte concentration along the channel, resulting in diffusioosmotic flow driven by the induced electric field and the induced pressure gradient. The induced electric field and pressure gradient are not uniform along the channel, and therefore, the diffusioosmotic flow is not fully developed. The major conclusions are

(i) When the bulk electrolyte concentration is relatively low, the fluids in the central region and in the region near the negatively charged wall flow, respectively, in the direction opposite to the applied concentration gradient and in the same direction as that of the concentration gradient. The net flow is in the direction of increasing electrolyte concentration. The flow rate decreases as the bulk concentration increases. This, however, is not true at high bulk electrolyte concentrations. Once the bulk electrolyte concentration exceeds a certain value, the fluid in the entire channel flows from one end with a higher electrolyte concentration to the other with a lower electrolyte concentration.

(ii) There is an optimal concentration gradient under which the flow rate attains a maximum. Below this optimal value, as the concentration gradient increases so does the net flow rate. Further increases in the concentration gradient above this critical value, the flow rate slightly decreases. The optimal concentration gradient is, among other things, a function of the surface charge density along the wall of the nanochannel.

(iii) When the bulk electrolyte concentration is relatively small, the flow rate increases with the increase in the magnitude of the surface charge density. However, the effects of the surface charge density on the flow rate are insignificant when the bulk electrolyte concentration is relatively high.

Acknowledgments

S.Q. acknowledges partial support from the National Science Foundation under Grant No. 0447416, and from UNLV NIA and PRA grants.

References

[1] R. Austin, Nature Nanotechnol. 2 (2007) 79.
[2] A. Van den Berg, M. Wessling, Nature 445 (2007) 726.
[3] A. De Leebeeck, D. Sinton, Electrophoresis 27 (2006) 4999.
[4] R. Mukhopadhyay, Anal. Chem. 78 (2006) 7379.
[5] J.C.T. Eijkel, A. Van den Berg, Microfluid. Nanofluid. 1 (2005) 249.
[6] D.C. Prieve, Adv. Colloid Interface Sci. 16 (1982) 321.
[7] D.C. Prieve, J.L. Anderson, J.P. Ebel, M.E. Lowell, J. Fluid Mech. 148 (1984) 247.
[8] H.J. Keh, J.H. Wu, Langmuir 17 (2001) 4216.
[9] H.J. Keh, Y.K. Wei, Langmuir 18 (2002) 10475.
[10] J.H. Wu, H.J. Keh, Colloids Surf. A Physicochem. Eng. Aspects 212 (2003) 27.
[11] Y.K. Wei, H.J. Keh, Colloids Surf. A Physicochem. Eng. Aspects 221 (2003) 175.
[12] Y.K. Wei, H.J. Keh, Colloids Surf. A Physicochem. Eng. Aspects 222 (2003) 301.
[13] H.J. Keh, H.C. Ma, Colloids Surf. A Physicochem. Eng. Aspects 233 (2004) 87.
[14] H.J. Keh, H.C. Ma, Langmuir 21 (2005) 5461.
[15] H.C. Ma, H.J. Keh, Colloids Surf. A Physicochem. Eng. Aspects 267 (2005) 4.
[16] H.C. Ma, H.J. Keh, J. Colloid Interface Sci. 298 (2006) 476.
[17] H.J. Keh, H.C. Ma, Langmuir 23 (2007) 2879.
[18] A. Ajdari, L. Bocquet, Phys. Rev. Lett. 96 (2006) 186102.
[19] R.F. Probstein, Physiochemical Hydrodynamics, Wiley, New York, 1994.
[20] S. Qian, A. Wang, J.K. Afonien, J. Colloid Interface Sci. 303 (2006) 579.
[21] H. Liu, S. Qian, H.H. Bau, Biophys. J. 92 (2007) 1164.
[22] D. Li, Electrokinetics in Microfluidics, Elsevier, New York, 2004.
[23] H. Daiguji, P. Yang, A. Majumdar, Nano Lett. 4 (2004) 137.
[24] A.V. Theemsche, J. Deconinck, B. Van den Bossche, L. Bortels, Anal. Chem. 74 (2002) 4919.
[25] P. Pivonka, D. Smith, Int. J. Numer. Methods Eng. 63 (2005) 1975.